# Toward the realization of subsurface volumetric integrated optical systems •

Cite as: Appl. Phys. Lett. **119**, 130503 (2021); https://doi.org/10.1063/5.0059354 Submitted: 08 June 2021 • Accepted: 11 September 2021 • Published Online: 01 October 2021

D Corey A. Richards, Christian R. Ocier, D Jinlong Zhu, et al.

### COLLECTIONS

F This paper was selected as Featured







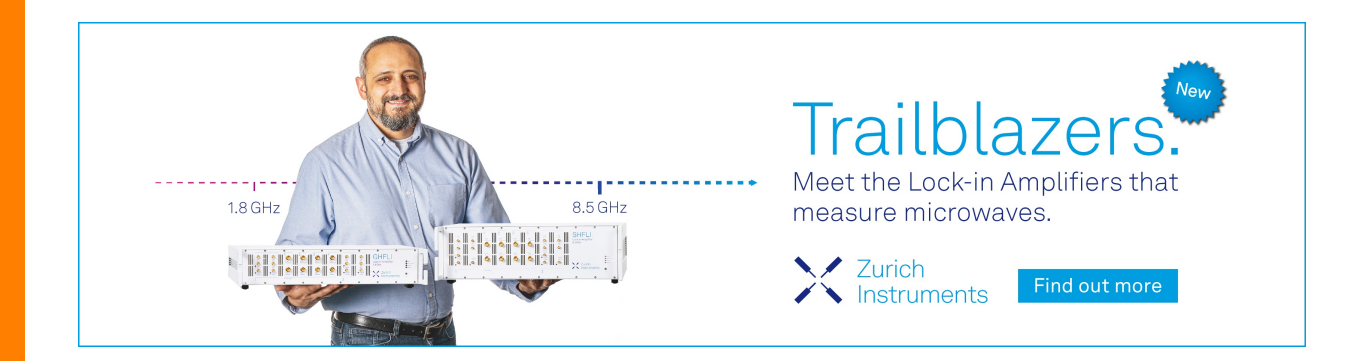
# **ARTICLES YOU MAY BE INTERESTED IN**

Prospects in x-ray science emerging from quantum optics and nanomaterials Applied Physics Letters 119, 130502 (2021); https://doi.org/10.1063/5.0060552

Nonlinear nanophotonics based on surface plasmon polaritons
Applied Physics Letters 119, 130501 (2021); https://doi.org/10.1063/5.0061726

Femtosecond laser direct writing continuous phase vortex gratings with proportionally distributed diffraction energy

Applied Physics Letters 119, 131101 (2021); https://doi.org/10.1063/5.0061590





# Toward the realization of subsurface volumetric integrated optical systems •

Cite as: Appl. Phys. Lett. **119**, 130503 (2021); doi: 10.1063/5.0059354 Submitted: 8 June 2021 · Accepted: 11 September 2021 · Published Online: 1 October 2021







Corey A. Richards, <sup>1,2,3</sup> (b) Christian R. Ocier, <sup>1,2,3</sup> (b) Jinlong Zhu, <sup>4,5,6</sup> (b) Lynford L. Goddard, <sup>3,4,5,a)</sup> (b) and Paul V. Braun<sup>1,2,3,7,a)</sup> (c)

### **AFFILIATIONS**

- Department of Materials Science and Engineering, University of Illinois Urbana-Champaign, Urbana, Illinois 61801, USA
- <sup>2</sup>Materials Research Laboratory, University of Illinois Urbana-Champaign, Urbana, Illinois 61801, USA
- <sup>3</sup>Beckman Institute for Advanced Science and Technology, University of Illinois Urbana-Champaign, Urbana, Illinois 61801, USA
- <sup>4</sup>Department of Electrical and Computer Engineering, University of Illinois Urbana-Champaign, Urbana, Illinois 61801, USA
- <sup>5</sup>Micro and Nanotechnology Laboratory, University of Illinois Urbana-Champaign, Urbana, Illinois 61801, USA
- <sup>6</sup>State Key Laboratory of Digital Manufacturing Equipment and Technology, Huazhong University of Science and Technology, Wuhan, China
- Department of Mechanical Science and Engineering, University of Illinois Urbana-Champaign, Urbana, Illinois 61801, USA

### **ABSTRACT**

Next generation mobile devices and computing architectures would benefit from ultra-high bandwidth technologies that efficiently transport and process optical signals. Subsurface fabrication can address this challenge by forming volumetric photonic integrated circuits with a more compact aerial footprint than planar on-chip circuits. These 3D optical systems may utilize densely packed low-loss, freeform optical interconnects for high volume data transfer. In this Perspective, we provide a comparative overview of the two main methods for subsurface fabrication, including our recently developed SCRIBE process, and assess the advantages and future directions of each approach. After analyzing the underlying technologies, we provide a roadmap of important steps to transition from laboratory demonstrations of individual elements to industrial-scale production of subsurface volumetric photonic integrated circuits.

Published under an exclusive license by AIP Publishing. https://doi.org/10.1063/5.0059354

# INTRODUCTION

Volumetric photonic integration avoids the limitations of traditional planar systems by utilizing all spatial degrees of design freedom. For example, networks of waveguide interconnects fabricated at multiple planes experience reduced interlayer communication losses and improved cross-sectional bandwidths by avoiding waveguide crossings and real estate limitations of single-layer photonic integrated circuits (PICs). A proven approach for stacking waveguides in three-dimensional (3D) space is to build up and encapsulate lithographically defined objects a layer at a time, with examples of multilayer waveguides shown in Figs. 1(a) (illustration) and 1(b) (experimental image). Layer-by-layer fabrication has also enabled the design of stacked meta-optics that target multiple wavelengths or perform dispersion correction as shown in Figs. 1(c) and 1(d), leading to compact achromats. However, encapsulated multilayer metaoptics are prone to errors in alignment and spacing layer thickness, leading to reduced

device performance.<sup>4,5</sup> Integrated systems formed via this approach also lack the ability to efficiently transport optical signals across multiple planes. Arbitrarily shaped volumetric interconnects that route light vertically, freeform refractive lenses and phase masks, and gradient refractive index (GRIN) optics are all excluded from this method's fabrication capabilities.

Here, we highlight the advantages of constructing 3D PICs using maskless direct-write fabrication, which seamlessly forms and integrates any configuration of optical components within 3D space. Direct-write subsurface fabrication methods use an ultrafast femtosecond pulsed laser to locally alter the properties of a medium, creating precisely positioned submicrometer voxels. The voxels are the building blocks of larger, more complex structures, and can be arranged into suspended lenses and waveguides that follow any optical path defined within a material's volume. We refer to a PIC that includes subsurface optics formed via maskless direct-write fabrication as a volumetric

<sup>&</sup>lt;sup>a)</sup>Authors to whom correspondence should be addressed: lgoddard@illinois.edu and pbraun@illinois.edu

# Layer-by-Layer Fabrication

# Waveguide Encapsulation Encapsulated Waveguides (a) Encapsulated Waveguides (b) Waveguide 2 SiO<sub>2</sub> Layer 3 SiO<sub>2</sub> Layer 2 SiO<sub>2</sub> Layer 1 Si 3 µm Encapsulated Nanoresonators Capping Layer Capping Layer Stacked Nanoresonators Stacked Nanoresonators Fused silica 500 nm

### **Direct-Write Subsurface Fabrication**

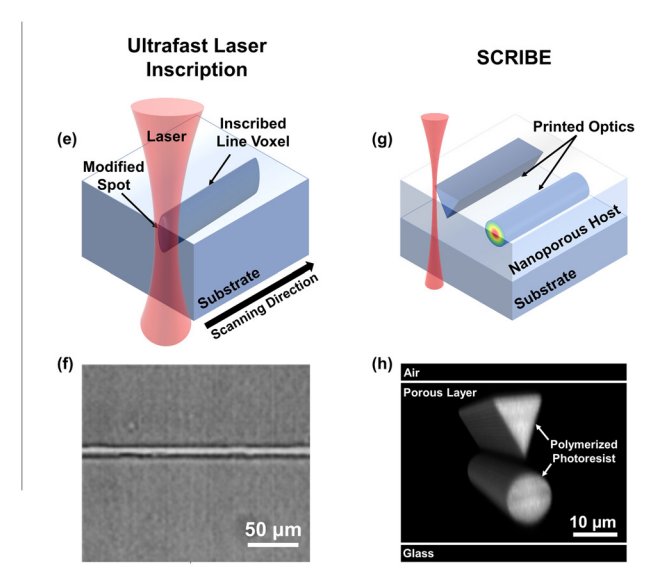


**FIG. 1.** (a) Illustration of multilayer encapsulated waveguides. Multiple planes of waveguides are lithographically defined and embedded within capping layers. (b) Scanning electron microscope (SEM) cross section of an encapsulated waveguide coupled to a ring resonator at a different plane. Waveguide 1 is encapsulated in SiO<sub>2</sub> layer 2, while waveguide 2 is in SiO<sub>2</sub> layer 3. Adapted with permission from Sherwood-Droz and Lipson, Opt. Express **19**(18), 17758 (2011). 1 Copyright 2011 The Optical Society. (c) Illustration of a multilayer encapsulated metaoptic. Multiple layers of nanoresonators are lithographically defined and embedded within capping layers. (d) SEM cross section of a bilayer metalens enabled by encapsulation in SU-8. Adapted with permission from Mansouree *et al.*, Optica **7**(1), 77 (2020). 25 Copyright 2020 The Optical Society. (e) Illustration of a waveguide or line voxel being formed inside a substrate using ultrafast laser inscription. A femtosecond pulsed laser is focused into the volume of a bulk material, such as glass, resulting in a region with a modified refractive index. Line voxels and waveguides are formed by scanning the laser in the desired pattern. (f) An optical image of a waveguide fabricated inside glass using ULI. Adapted with permission from Miura *et al.*, Appl. Phys. Lett. **71**, 3329 (1997). 10 Copyright 1997 AIP Publishing LLC. (g) Illustration of optics being formed using SCRIBE. A femtosecond pulsed laser selectively polymerizes a nonlinear photoresist within the pores of a nanoporous layer. Single index optics are formed by keeping laser conditions constant during printing, while GRIN optics are formed by continuously varying the laser exposure during printing. (h) Fluorescence intensity scan of a prism and a cylinder printed inside a porous silicon film using SCRIBE. The two geometries are naturally aligned during the writing process and separated with a 3 μm gap where no photoresist is polymerized.

photonic integrated circuit (VPIC). The ultimate goal of VPICs is to interface compact subsurface optics with traditional on-chip devices and electronics for enhanced signal routing and interlayer communication. In this Perspective, we highlight the two most prominent modes of direct-write subsurface fabrication: ultrafast laser inscription (ULI) [Figs. 1(e) and 1(f)] and subsurface controllable refractive index via beam exposure (SCRIBE) [Figs. 1(g) and 1(h)]. We examine the key differences between the approaches and provide a roadmap for advancing the adoption of VPIC technology.

Freeform subsurface optics were first created by using a focused femtosecond pulsed laser to locally modify the refractive index of glass<sup>8,9</sup>—a technique referred to as ULI. Scanning a laser in the desired pattern results in the formation of high aspect ratio 3D structures inside the volume of substrates including glass, <sup>10</sup> silicon, <sup>11</sup> and some polymers. <sup>12–14</sup> Although the refractive index change between the modified spot and the surrounding medium is small ( $\Delta n \approx 0.001$ –0.06), <sup>12,15,16</sup> ULI has been used to fabricate 3D diffractive optical elements (DOEs) <sup>11,17,18</sup> and to promote low-loss transmission through subsurface waveguide devices. <sup>7,19–22</sup> Figure 1(e) shows how ULI is used to form subsurface line voxels and waveguides. An optical image of a waveguide experimentally formed inside silica via ULI is provided in Fig. 1(f).

More recently, a diversity of subsurface optics that manipulate and guide light have been enabled by SCRIBE's combined submicrometer control over the geometry and optical properties of fabricated structures.<sup>6</sup> Like ULI, SCRIBE uses a femtosecond pulsed laser to write 3D optical components within a medium. However, SCRIBE uses the laser to selectively polymerize a photoresin within a porous scaffold rather than altering the host material's properties. The local effective refractive index of SCRIBE-printed optics can be tuned over an unprecedented continuous range of  $\Delta n \approx 0.41$  by adjusting laser power, scan speed, and voxel density during printing, with a maximum index contrast of around 0.6 between the printed structure and the surrounding medium. The porous host locks printed voxels in place, and therefore, multilayer elements and compound optics formed with SCRIBE have precise lateral alignment and vertical offsets. SCRIBE can render both single index and GRIN optics as depicted in Fig. 1(g). Figure 1(h) shows a fluorescence image of the geometries from Fig. 1(g) that have a vertical gap of 3 μm. Porous silicon (PSi) and porous silica (PSiO<sub>2</sub>) are currently preferred as SCRIBE-scaffolds due to their low absorptions at key wavelengths and their ability to host secondary materials, 23,24 but the use of other host materials may also be possible.

# **ULTRAFAST LASER INSCRIPTION**

ULI has demonstrated low-loss waveguides inside various substrates, with propagation losses as low as  $0.15\,\mathrm{dB/cm}$  at  $1.55\,\mu\mathrm{m}$  inside silica. <sup>21</sup> Fully 3D passive devices that are challenging to fabricate and

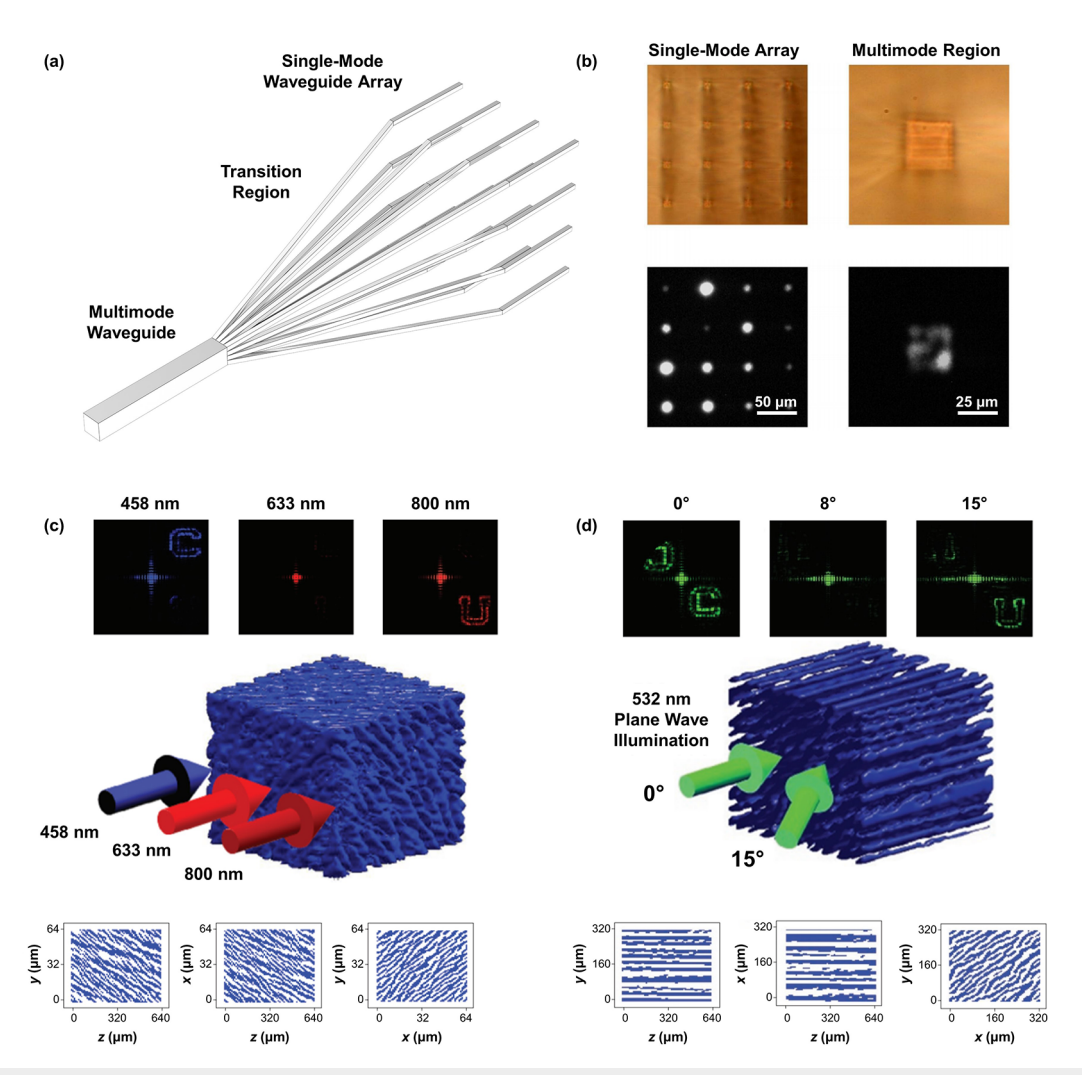


FIG. 2. (a) Sketch of the 3D MM-SM transition region in an integrated photonic lantern. The transition region connects a multimode waveguide to a single-mode waveguide array. (b) White light transmission optical micrographs (top) and a near field image of the photonic lantern injected with 1539 nm light (bottom) in the SM and MM regions. Panels (a) and (b) adapted with permission from Thomson et al., Opt. Express 19(6), 5698 (2011).<sup>26</sup> Copyright 2011 The Optical Society. (c) Wavelength multiplexed volume DOE that produces different diffraction patterns for different wavelengths. (Middle) A 3D rendering of the volume DOE. (Bottom) Isometric projections of the volume DOE's structure. (d) Angular multiplexed volume DOE that produces different diffraction patterns for different angles. (Middle) A 3D rendering of the volume DOE. (Bottom) Isometric projections of the volume DOE's structure. Panels (c) and (d) adapted with permission from Gerke and Piestun, Nat. Photonics 4, 188 (2010).<sup>17</sup> Copyright 2010 Springer Nature.

scale through traditional methods have been enabled by this approach. One such device is the photonic lantern [Fig. 2(a)], which couples light from a multimode (MM) waveguide to a single-mode (SM) waveguide array and vice versa. Photonic lanterns are primarily used to filter and remap light collected by telescopes for stellar interferometry, but more generally convert between MM and SM waveguides as required by the optical system under consideration. Photonic lantern that converts a MM waveguide to a  $4 \times 4$  SM waveguide array was demonstrated using ULI with an insertion loss of approximately 4 dB for one MM-SM-MM transition and a straight section propagation loss of 0.7 dB/cm. Transmission micrographs and near field images of the photonic lantern's cross section at the MM and SM regions are shown in Fig. 2(b). There are various strategies to further reduce losses in

inscribed waveguiding devices. For example, the photonic lantern design was improved by using a multicore design for the MM region and optimizing the MM-SM transition length. These changes resulted in a MM-SM-MM throughput of 75% (1.25 dB of loss, compared to the previous loss of 4.0 dB).<sup>28</sup> The throughput of the device was further improved to greater than 95% by optimizing the pitch between the waveguides in the MM section to ensure that the total number of modes supported by the MM and SM sections nearly matched.<sup>28</sup>

The MM-SM transition length of the updated photonic lantern was varied between 1 and 10 mm, with the lowest loss occurring at 5 mm. <sup>28</sup> However, 3D devices with micrometer-scale footprints are required for the ultracompact VPICs that we envision. To further miniaturize subsurface waveguiding devices, it is necessary to investigate

new substrate materials that can support higher index contrasts between the waveguide and surrounding medium, permitting smaller bending radii and smaller cross-sectional dimensions. Polymers are another class of materials that have been demonstrated to be capable of supporting 3D ULI-written waveguides with high quality and low propagation losses, 12,29 which show promise for further miniaturization. As a first step, it was shown that an index modification of around 0.004 in polymers, such as polymethyl methacrylate (PMMA), occurs from depolymerization, cross-linking, and densification induced by the ultrafast laser. 30-32 Alternatively, a photosensitive monomer can be infiltrated within the matrix of another polymer,<sup>33</sup> recently leading to a much higher index contrast of 0.06 by permeating phenylacetylene inside polydimethylsiloxane (PDMS) and then using ULI to selectively polymerize the infilled monomer. 12 A small cross-sectional radius of 1.3  $\mu$ m and a low transmission loss of 0.03 dB/cm in the 650–700 nm range were achieved by the PDMS-supported 3D waveguides. Although these waveguides may be useful for connecting two distant devices on an integrated chip, index contrasts that significantly exceed 0.06 are still required to achieve ultracompact 3D devices.

The spatial control afforded by subsurface fabrication also allows ULI to be directed toward the formation of arbitrarily patterned DOEs. As a demonstration, aperiodic DOEs that perform wavelength [Fig. 2(c)] and angular [Fig. 2(d)] multiplexing were fabricated inside glass using ULI.<sup>17</sup> The first DOE outputs a diffraction pattern in the shape of the letter C or U for different wavelengths (458 or 800 nm) [Fig. 2(c)], while the second DOE produces the C and U-shaped patterns at different angles (0° or 15° at 532 nm) [Fig. 2(d)]. These volumetric DOEs showcase the ability of subsurface fabrication to generate optical elements that traditional approaches are incapable of forming. However, the highlighted DOE is a binary refractive index element

with a low refractive index contrast, resulting in a maximum scattering efficiency of only 12%. <sup>17</sup> Like ULI-fabricated waveguides, developing a method of forming high index contrast voxels with continuously tunable GRIN profiles over a high dynamic range would lead to more efficient volumetric DOEs. Improved refractive index control may also enable the formation of 3D GRIN waveguides, phase masks, and lenses.

The incorporation of functional materials into substrates is a significant step toward expanding subsurface fabrication capabilities to include active devices. Recently, the 3D printing of metal halide perovskite quantum dots was demonstrated inside the volume of bulk glass [Fig. 3(a)].<sup>34</sup> Doping the glass with Cs, Pb, and Br elements allowed for the in situ formation of CsPbBr3 quantum dots by using a femtosecond pulsed laser to supply the necessary energy to form quantum dots at the focal spot, where the local photoluminescence is controlled by adjusting the laser exposure [Fig. 3(b)]. Due to the ionic structure and the low formation energy of CsPbBr<sub>3</sub> quantum dots, the laser can also be used to decompose previously printed structures, enabling key applications, such as reprogrammable data storage. Furthermore, restoration of erased structures is accomplished through annealing [Fig. 3(c)]. Future research should extend this quantum dot fabrication method to other functional materials and integrate laser patterned metal halide perovskite quantum dots into subsurface active devices.

### **SCRIBE**

SCRIBE can support index contrasts as high as roughly 0.6 between the polymerized region and surrounding medium, 6 leading to the formation of 3D waveguides with significantly smaller bending radii than ULI. The fluorescence image in Fig. 4(a) shows a SCRIBE-rendered single-mode waveguide with a bending radius of  $18.5 \, \mu m$ 

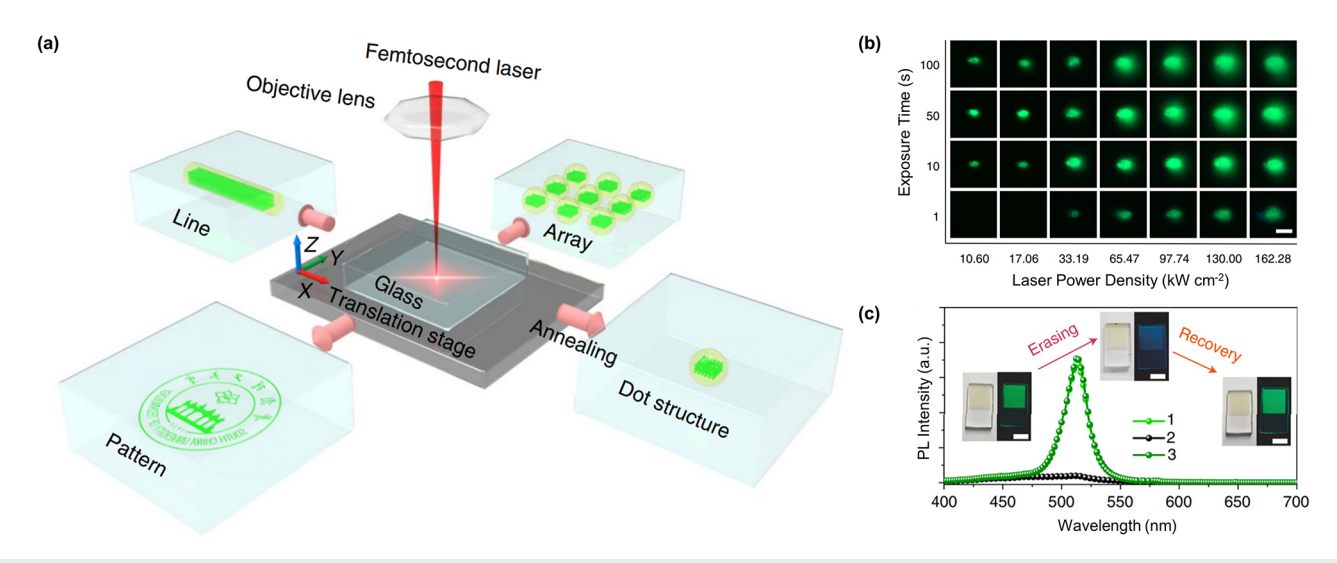
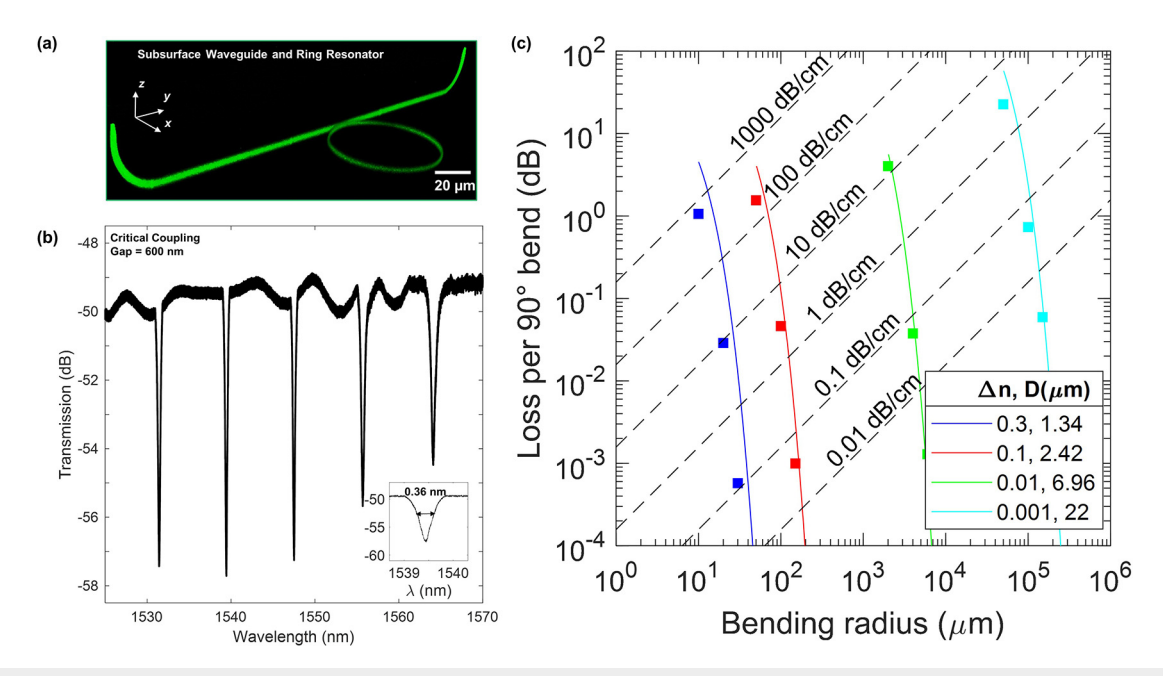


FIG. 3. (a) Illustration of volumetric photoluminescent structures that can be formed inside glass by subsurface laser patterning of quantum dots. By scanning a femtosecond pulsed laser in the desired pattern, line structures, artwork, complex structures, and arrays of structures can be formed from quantum dots. The green color signifies photoluminescence. (b) Laser exposure-dependent size and fluorescence of subsurface quantum dots under 365 nm light. More quantum dots are formed at high laser power densities and exposure times, resulting in higher photoluminescence. Scale bar, 50  $\mu$ m. (c) Decomposition and recovery of printed subsurface quantum dots. The graph shows the photoluminescence spectra of the subsurface quantum dots after printing (line 1), after erasing (line 2), and after recovering the erased structure by annealing (line 3). Picture insets show optical images of printed structures under ultraviolet excitation through one cycle of laser patterning, erasing, and recovering. High photoluminescence is observed after patterning and recovery, but not after erasing. Scale bars, 3 mm. Panels (a)–(c) adapted with permission from Huang et al., Nat. Photonics 14, 82 (2020).<sup>34</sup> Copyright 2020 Springer Nature.



**FIG. 4.** (a) Fluorescence intensity image of a single-mode subsurface waveguide coupled to ring resonator printed inside PSiO<sub>2</sub> using SCRIBE. The bending radii of the input and output ports are  $18.5 \,\mu\text{m}$ . The bending radius of the ring resonator is  $30 \,\mu\text{m}$ . The cross-sectional diameter is roughly  $1 \,\mu\text{m}$ . (b) Measured microring resonator spectrum for the critically coupled condition operating in TE mode. The inset shows a resonance full width at half maximum (FWHM) of 0.36 near  $1539.5 \,\text{nm}$ . Panels (a) and (b) adapted with permission from Ocier *et al.*, Light Sci. Appl. **9**, 196 (2020). Copyright 2020 Authors, licensed under a Creative Commons Attribution (CC BY 4.0) license. (c) Graph of bending loss vs bending radius for single-mode step-index zero-propagation loss waveguides with different index contrasts and cross-sectional diameters at  $1550 \,\text{nm}$ . For a fair comparison, the core diameter was adjusted to keep the V-number fixed at 2.4, i.e., just below the cutoff of 2.405 for single-mode operation. The solid squares are from 20 axisymmetric COMSOL simulations using the Wave Optics module, and the solid lines are calculated curves using the approximate equations for weakly bent fiber (Ref. 14). The COMSOL simulations were built upon the model (Ref. 36) with adaptations that ensured convergence and proper mode selection as the device parameters changed. The effective indices used for the approximate equations were obtained through COMSOL simulations of straight fibers. For the green and cyan curves and data points, an  $5iO_2$  cladding with an index of 1.44 was assumed, as is typical for ULI. The red and blue curves and data points assumed a cladding index of 1.15, which is the index of the PSiO<sub>2</sub> scaffold used to hold SCRIBE-printed optics. The black dashed lines represent the propagation loss, which is added to the bending loss to get the total loss.

and a diameter of 1  $\mu$ m, which was critically coupled to a 30  $\mu$ m radius microring resonator.<sup>6</sup> The measured microring spectrum in Fig. 4(b) displays a quality factor (Q) of up to 4310 in the telecom C-band. The high 50 dB insertion loss is primarily due to the enormous modal mismatch from direct coupling between the 8  $\mu$ m diameter fiber core and the 1  $\mu$ m diameter waveguide core at the input and output ports. By adding subsurface lenses, the total insertion loss for the fiber-coupled 3D waveguide with 25  $\mu$ m bending radii and 528.5  $\mu$ m total length was drastically improved to 10.9 dB. 35 This total loss includes coupling, bending, propagation, and stitching error losses. Detailed experiments and analyses are required to determine the relative contributions of these losses and how they each vary with laser writing conditions and waveguide geometry. This information will play a critical role in determining appropriate applications for SCRIBE-written 3D waveguides. Nevertheless, the dramatic reduction in footprint is a significant step toward realizing ultracompact VPICs.

As subsurface fabrication technology develops, it is important to quantify the compactness of a VPIC given the achievable index contrast. Figure 4(c) highlights the importance of index contrast and provides an initial pathway for low-loss 3D waveguide design. In this graph, the color symbols (COMSOL Wave Optics simulation) and solid lines (approximate theoretical model<sup>14</sup>) show bending loss vs

bending radius of single mode waveguides with different index contrasts. There is general agreement for the ranges shown, but the assumptions in the theoretical model fail at smaller radii and the COMSOL model does not find the real part of the eigenvalues accurately enough to extract the loss at larger radii. The black dotted lines show the propagation losses for a given value in units of dB/cm. The total loss of a given waveguide bend is the sum of the appropriate color symbol or line and the black dotted line. The data shown in green and cyan represent the waveguide index contrasts and diameters obtainable by ULI, and the data in red and blue represent values easily achievable with SCRIBE.

The bending losses experienced by ULI-waveguides increase drastically as the bending radius decreases to 1 mm, while the waveguides formed by SCRIBE retain low bending losses for radii as small as  $10\,\mu\text{m}$ . Figure 4(c) can be used to calculate the number of bends achievable for a given index contrast, propagation loss, and maximum permissible loss of the waveguide in dB. For example, if a designer has a total permissible loss of 3 dB, then an index contrast of 0.3 and a propagation loss of 1 dB/cm would allow for fifty  $20-\mu\text{m}$  bends (using the COMSOL value) and  $1.34\,\text{cm}$  of straight waveguide sections. Meanwhile, an index contrast of 0.01 and the same 3 dB loss budget and 1 dB/cm propagation loss would only allow for two or three mm-scale

bends and less than 1 cm of straight waveguide section. Thus, SCRIBE has the potential to generate densely arrayed fiber-coupled 3D waveguide interconnects as highlighted by this first example.

Future SCRIBE research should prioritize reducing the interconnect loss mechanisms for lower loss light routing through volumetric space. The current hypothesis is that reflections at various interfaces, stitching errors during writing, line edge roughness from galvoscanning the voxel lines, scattering at the pore-wall interface, and bending losses all contribute to the measured 10.9 dB of insertion loss. Investigations of subsurface GRIN anti-reflection (AR) coatings, the writing tool and the polymerization process, adoption of sidewall smoothing techniques (e.g., resist reflow, multipass writing, and concentric GRIN cladding layers), use of alternate host materials with finer pores, and optimizing the waveguide diameter for a given index contrast to operate with a V-number closer to 2.4 are several research directions that address these respective issues.

Subsurface lens design is crucial for coupling light into 3D interconnects across multiple planes. SCRIBE can manufacture subsurface lenses with high geometric fidelity and tunable optical properties. As an early exploration of SCRIBE's lens forming capabilities, a multilayer doublet that performs chromatic correction across visible wavelengths was rendered inside PSi.<sup>6</sup> A fluorescence scan of the subsurface achromat is shown in Fig. 5(a). The regions of different fluorescence intensities correspond to different polymer fill fractions and, therefore, different refractive indices and Abbe numbers. The chromatic focal curve in Fig. 5(b) shows how these parameters can be fine-tuned to control the focal lengths for visible wavelengths by comparing the doublet to two different types of singlets. Unlike achromats formed by encapsulation, multilayer SCRIBE-generated optics are formed in a single printing step and, therefore, offer precise spatial positioning. These advantages mean that future dispersion-engineered optics printed with SCRIBE may include multilayer DOEs as well as refractive optics.

SCRIBE not only offers higher index contrasts than ULI, but it can also form GRIN structures with precisely controlled indices over a range of 0.41.<sup>6</sup> The high contrast tunable index has been utilized to form the world's smallest spherical Luneburg lens [cutaway diagram in Fig. 5(c)].<sup>6</sup> Luneburg lenses that focus infrared (IR) frequencies were previously demonstrated using 3D printed metamaterials. The effective refractive index profile within the metamaterial lens was

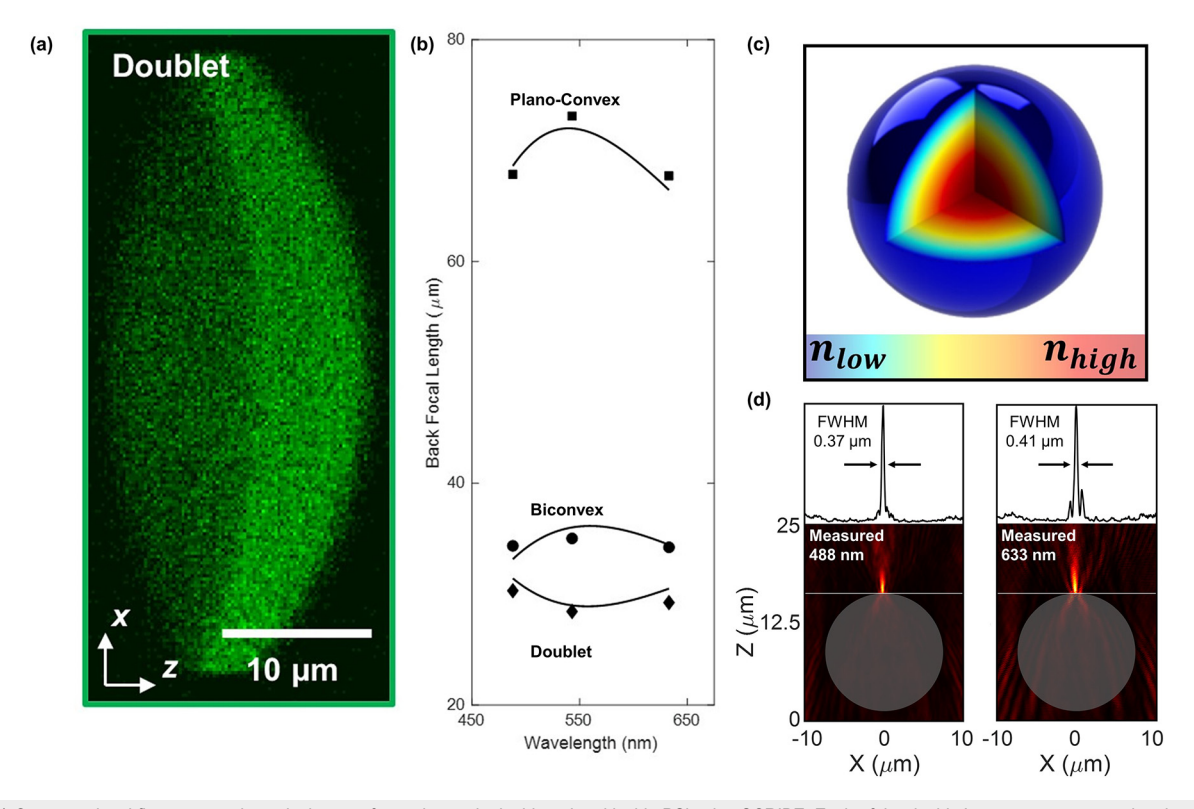


FIG. 5. (a) Cross-sectional fluorescence intensity image of an achromatic doublet printed inside PSi using SCRIBE. Each of the doublet's components was printed under different laser conditions, as indicated by the regions of different fluorescence intensities. The distinct regions exhibit different refractive indices and Abbe numbers. (b) The measured focal lengths of the printed achromat in (a) at different wavelengths (diamonds). The solid curve depicts the focal lengths simulated using Zemax. The other two curves represent plano–convex and biconvex singlets for comparison. (c) Cutaway schematic of a spherical Luneburg lens. The refractive index gradually increases from edge to center according to the equation:  $n(r) = n_{surface} - n_{air} + \sqrt{2 - (\frac{r}{R_{loss}})^2}$ . (d) A confocal intensity scan of SCRIBE-printed Luneburg lenses focusing 488 nm (left) and 633 nm (right) light to their opposite surfaces. The horizontal white line represents the interface between air and the porous silicon film. The SCRIBE-Luneburg lenses have 15  $\mu$ m diameters. Panels (a)–(d) adapted with permission from Ocier *et al.*, Light Sci. Appl. 9, 196 (2020). Copyright 2020 Authors, licensed under a Creative Commons Attribution (CC BY 4.0) license.

spatially modulated by creating unit cells with different fractions of polymer and air.<sup>37</sup> However, the minimum unit cell size is limited by the resolution of the fabrication technique, preventing further miniaturization. SCRIBE-rendered GRIN structures do not employ the unit cell design approach, leading to Luneburg lenses that focus wavelengths as low as 488 nm (limited by the wavelengths available in the measurement equipment). Confocal scans of SCRIBE-printed Luneburg lenses focusing 488 and 633 nm light are shown in Fig. 5(d).

Other SCRIBE-printed GRIN optics include flat parabolic lenses, flat axicons, flat Airy beam phase masks, and cylindrical lenses with arbitrary index profiles.<sup>6,38</sup>

# **FUTURE DIRECTIONS**

Fully realized VPICs will combine many different optical elements, electronics, and active devices into a single volume with ultrahigh density. Figure 6(a) provides an artistic rendering of an

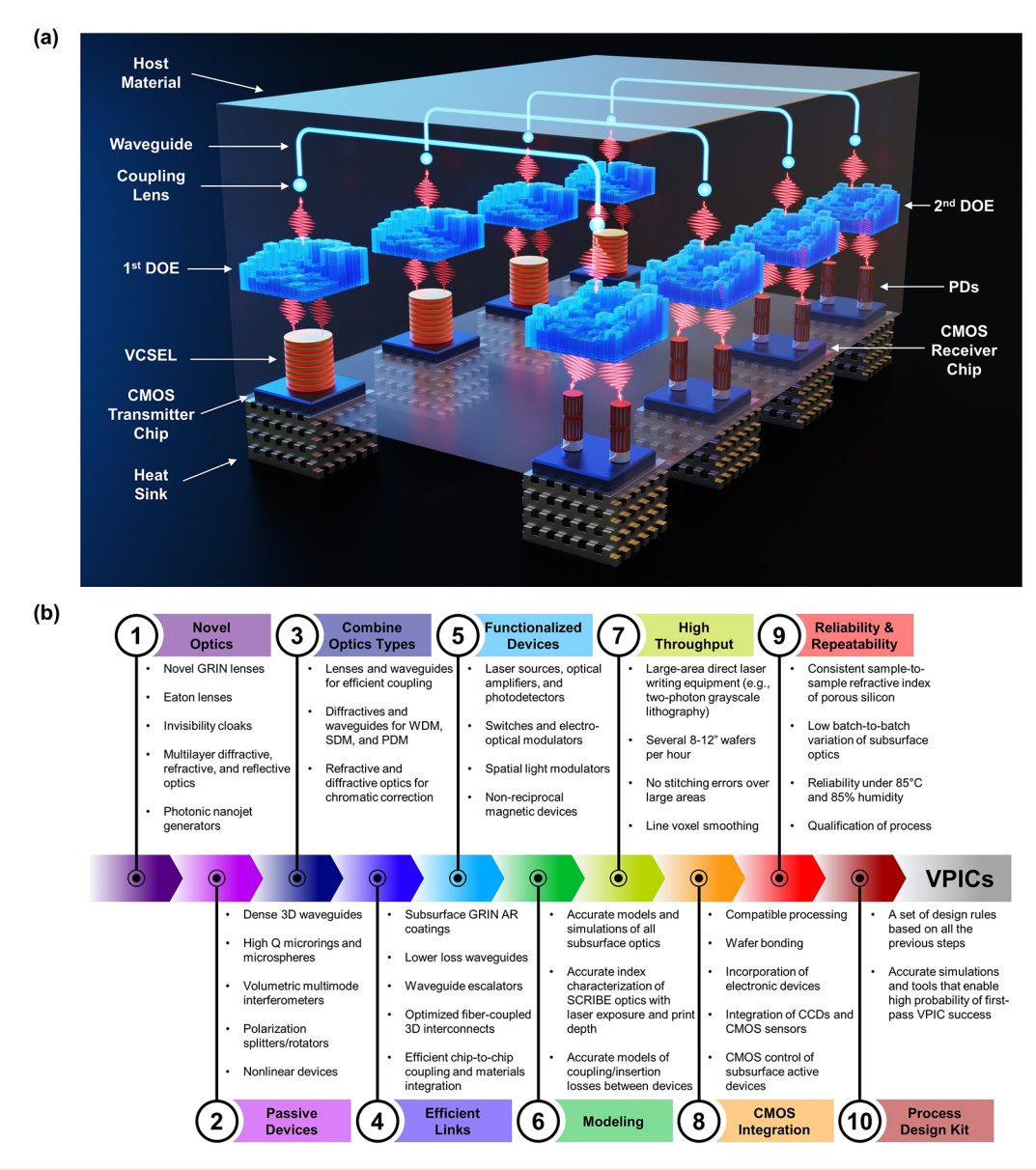


FIG. 6. (a) Envisioned optical interposer VPIC. Each of the four independent CMOS transmitter chips sends a data signal or a clock signal as light to multiple locations on the respective CMOS receiver chip. The VPIC has VCSELs for optical encoding and PDs for decoding. Each VCSEL includes a DOE acting as an external cavity mirror that fixes the wavelength and spatial mode. The light is then focused by a coupling lens into a waveguide and collimated again on the other side. The DOE above each CMOS receiver chip splits the light and equally distributes the signal to the output PDs. (b) A roadmap leading from laboratory-scale demonstrations of subsurface optics to the completion of a fully functional VPIC system. Steps 1–6 can be more easily researched in an academic setting. Steps 7–10 are necessary for the mass production of VPICs and may require industrial research and development to complete.

envisioned futuristic optical interposer VPIC that uses diffractive, refractive, and waveguiding elements to carry signals from a vertical cavity surface emitting laser (VCSEL) array to a photodetector (PD) array across 3D space. The first DOE forms an external cavity that fixes the wavelength and spatial mode of the light emitted by a VCSEL. A lens above the DOE couples the light into a 3D waveguide, which transports the signal to a second lens that collimates the output. A second DOE then equally distributes the output signal among all the PDs on the complementary metal–oxide–semiconductor (CMOS) receiver chip. The illustration represents one small section of a larger VPIC. The envisioned system would contain vast arrays of VCSELs and PDs with thousands of interconnects transporting signals through an intertwined network of 3D waveguides between the chips.

Figure 6(b) provides a roadmap toward widespread adoption of VPICs. It details key steps toward the realization of 3D integrated systems like the one in Fig. 6(a). First, the library of subsurface optical devices and sub-systems that can be fabricated should be expanded [Fig. 6(b) steps 1–6]. Volumetric GRIN writing capabilities may enable the demonstration of novel freeform optical elements, including micro-scale Eaton lenses and invisibility cloaks that steer light across three dimensions. Stacked echelette gratings with optimized geometries and refractive indices could be used for high efficiency light manipulation and wavelength splitting. <sup>39</sup> Other stacked and GRIN optics, such as nanojet generators, would permit super-resolution imaging and coupling into extremely thin waveguides. <sup>40</sup>

The freeform 3D topology of direct-write fabrication should also be leveraged to form additional volumetric passive devices beyond the ones that have previously been demonstrated with ULI (e.g., photonic lanterns). Subsurface high Q microspheres, multimode interferometers, and polarization splitters and rotators should all be explored. Moreover, different types of optics should also be combined to form compound devices with advanced functionalities. For example, the availability of suspended waveguides and refractive, reflective, and diffractive optics in a single platform [as highlighted by Fig. 6(a)] may enable ultrahigh density and bandwidth 3D wavelength division multiplexing (WDM), space division multiplexing (SDM), and polarization division multiplexing (PDM) sub-systems with many input/output channels (e.g., arranged in 2D arrays). Additionally, light concentrators and resonant structures may permit nonlinear applications, such as optical digital signal processing or machine learning.

Efficient optical links are essential for communication between VPIC devices and for interfacing with external systems. Minimizing propagation losses, bending losses, and reflections at interfaces will be needed for low-loss connections. Waveguide escalators (e.g., S-bend 3D waveguides) can transport light vertically between the planes of a VPIC. As VPICs transition from small-scale laboratory demonstrations into commercial use, the demonstration of efficient in-chip, fiber-to-chip, and chip-to-chip links becomes more important. Figure 6(a) emphasizes the role diffractive and refractive optics may have for increasing the efficiency of 3D optical interconnects.

In addition to combining multiple types of elements to form passive devices and to achieve efficient links, subsurface optics should be combined with different types of materials to gain new functions. The laser-induced formation of photoluminescent materials has already been demonstrated using ULI,<sup>34</sup> marking the first step toward the design of active subsurface devices. Functional materials can also be infilled into the pores of SCRIBE scaffolds or used to dope photoresists

for SCRIBE printing. For instance, selectively filling the pores of PSi with active materials like quantum dots or dye-gain materials could allow for in-chip laser devices, optical amplifiers, and photodetectors, while filling the pores with liquid crystals could lead to electro-optic modulators, switches, attenuators, and spatial light modulators (SLMs). The fabrication of in-chip Faraday rotators for passive optical isolation<sup>41</sup> may also be made possible by infilling the pores or doping a substrate with magnetic materials. Optical isolators and circulators composed of fully 3D subsurface components may handle higher optical powers than their on-chip counterparts by spreading out the light within the volume. Previously, doped and specialized photoresists have been used to demonstrate laser-induced assembly of composite quantum dot emitters<sup>42</sup> and liquid crystal actuators. <sup>43</sup> Carrying out this process inside the pores of a scaffold material could make the discussed active devices a reality.

All the subsurface optical elements and devices discussed require highly accurate models, especially those formed with SCRIBE. SCRIBE currently uses PSi and PSiO<sub>2</sub> as scaffolding materials, which exhibit depth-dependent refractive indices and extinction coefficients due to the porosification process. While this phenomenon can be easily modeled using ellipsometry, the refractive index and voxel size of a polymerized photoresin also vary with print depth. The laser dosage delivered to a given plane is not precisely known because the extinction coefficient follows a depth-dependent gradient. Therefore, a simple analytic equation cannot adequately describe the voxel size or index. Extremely precise empirical data fitting or machine learning-assisted ellipsometry models may be necessary to fully characterize SCRIBE-printed structures. Once SCRIBE-printed structures are better characterized and modeled, system level models will become more accurate.

Subsurface optics are generally fabricated from the bottom-up to avoid wavefront distortions that may occur from writing through previously formed features. We have successfully printed at a depth of  $60\,\mu\mathrm{m}$  in PSiO $_2$  and  $25\,\mu\mathrm{m}$  in PSi. The PSiO $_2$  print depth is currently limited only by the thickness of PSiO $_2$  that we can produce. The small amount of absorption in PSi ( $\alpha\sim15\,\mathrm{cm}^{-1}$  for the previously used pulsed laser with a wavelength of  $780\,\mathrm{nm})^6$  makes printing deeper than  $25\,\mu\mathrm{m}$  more challenging. The maximum depth may be extended further by the increasing laser exposure as a function of print depth (which requires more accurate models) or by using light of a slightly longer wavelength ( $\alpha\sim10\,\mathrm{cm}^{-1}$  at  $800\,\mathrm{nm})^6$  or even beyond the bandgap of Si to ensure complete transparency. The print depth cannot exceed the working distance of the objective, so a longer working distance objective with a lower numerical aperture may be required for printing VPICs deep inside a porous medium.

To transition from laboratory demonstrations to industrial production, the throughput of subsurface fabrication needs to be greatly increased. Masked fabrication approaches, such as deep and extreme ultraviolet lithography, can produce >100 twelve-inch wafers per hour. Heaville, most current maskless direct-write equipment used by ULI and SCRIBE are incapable of printing a single two-inch wafer per hour, largely due to the time consuming processes of serial single-beam writing and using mechanical translation to stitch together writing fields (typically  $150\times150\,\mu\text{m}^2$  for high resolution printers). Furthermore, ULI and SCRIBE are often used to print volumetric elements, which naturally take longer to produce than a single layer, as in masked lithography. Projection micro-stereolithography (P\$\mu SL) offers an initial step toward solving this drawback by using a

dynamic mask to simultaneously polymerize two-dimensional layers in a single exposure. A fabrication speed of  $24.54\,\mathrm{mm}^3$  per hour was demonstrated (a roughly  $14\,000$ -fold improvement in writing speed compared to direct laser writing) at the cost of submicrometer resolution. We envision using  $P\mu\mathrm{SL}$  to make large volume elements in conjunction with femtosecond pulsed laser manufacturing for structures that require smaller features. Additionally, equipment with independently controllable parallel writing heads (e.g., by incorporating multiple femtosecond laser sources or SLMs to split the light of one or more significantly higher power laser sources) may improve throughput without sacrificing resolution.

Subsurface fabrication processes that are compatible with the CMOS process and with electronic devices like charge-coupled devices (CCDs) and CMOS image sensors must also be developed. PSi must be converted into PSiO<sub>2</sub> to support low-loss SCRIBE-printed waveguides (typically by dry thermal oxidation at 900 °C for 30 min). Therefore, a process where PSiO<sub>2</sub> can be formed without damaging other devices is necessary. Some possible solutions include oxidizing the PSi at lower temperatures for longer times and high-pressure wet oxidation. However, these approaches may still not be compatible with many electronic components. Combining SCRIBE with encapsulation may solve the compatibility issue, as PSi and PSiO2 can be readily transferred onto polymer substrates that have high enough adhesion. 48,49 CMOS chips can be embedded in a polymer while SCRIBE processing is done separately. The SCRIBE-printed components can then be aligned to the CMOS chip and transferred onto the polymer substrate. This approach does not solve the issue of establishing electrical connections; thus, additional engineering is needed.

Reliability and repeatability are especially important for SCRIBE, which uses materials that are known to show inconsistencies in their properties when created in different labs and in different environments, meaning that extremely strict standards are required for large-scale use of SCRIBE.<sup>50</sup> The ability of SCRIBE-generated VPICs to retain their specified properties for long periods of time is also important because the refractive index of unoxidized PSi has also been shown to slowly change as the silicon is oxidized.<sup>50</sup> This issue is worsened if the PSi is used in a humid environment, making a way to keep out moisture essential. Foundry-specific processes that result in low batch-to-batch variation are also vital.

The final step toward commercial adoption of VPICs is the creation of process design kits (PDK). PDKs are a collection of rules, tools, and simulation packages to assist customers with creating personalized integrated circuit designs. Accurate characterization, modeling, and compatible fabrication steps are necessary to develop PDKs. Once steps 1–9 of Fig. 6(b) are thoroughly addressed, PDKs for subsurface optics can be developed and VPICs may become widely used.

## **SUMMARY**

In summary, direct-write fabrication platforms present a pathway toward the development of ultracompact volumetric optical systems. Using a femtosecond pulsed laser to arrange voxels in 3D enables the manufacturing of arbitrarily integrated photonic structures in a single lithographic step. Devices written directly inside the volume of a substrate are protected and supported by the host medium, resulting in a simplified design approach that does not require additionally fabricated scaffolding structures. We have examined the advantages, disadvantages, and prospects of the two prominent methods for subsurface

fabrication—ULI and SCRIBE. ULI-fabricated waveguides can carry optical signals long distances within a chip and are appropriate for systems that have strict propagation loss requirements. SCRIBE, on the other hand, forms high index contrast waveguides with low bending losses and seamlessly integrates them with diffractive and refractive components. Several advancements in the underlying technology are required for the widespread adoption of subsurface volumetric integrated systems, such as increasing the index contrast of ULI waveguides, decreasing the losses of SCRIBE interconnects, forming subsurface active devices, and establishing subsurface electrical contacts. High throughput techniques also need to be established and tested for industrial-scale production of subsurface VPICs. Once these challenges are addressed, we believe that subsurface fabrication will revolutionize optical design and photonic integration.

# **ACKNOWLEDGMENTS**

This work was supported by a University of Illinois Urbana-Champaign College of Engineering Strategic Research Initiative, the National Science Foundation (No. ECCS-1935289), and the United States Department of Defense through the National Defense Science and Engineering Graduate (NDSEG) Fellowship Program.

### **AUTHOR DECLARATIONS**

### **Conflict of Interests**

L. L. Goddard, P. V. Braun, J. Zhu, C. H. Ocier, and C. A. Richards claim a U.S. patent on some of the processes and devices presented in this work through the University of Illinois Urbana-Champaign.

# **DATA AVAILABILITY**

The data that support the findings of this study are available from the corresponding authors upon reasonable request.

# **REFERENCES**

- <sup>1</sup>N. Sherwood-Droz and M. Lipson, "Scalable 3D dense integration of photonics on bulk silicon," Opt. Express **19**, 17758–17765 (2011).
- <sup>2</sup>R. T. Chen, L. Lin, C. Choi, Y. J. Liu, B. Bihari, L. Wu, S. Tang, R. Wickman, B. Picor, M. K. Hibb-Brenner, J. Bristow, and Y. S. Liu, "Fully embedded board-level guided-wave optoelectronic interconnects," Proc. IEEE 88, 780–793 (2000).
- <sup>3</sup>Y. Zhou, I. I. Kravchenko, H. Wang, H. Zheng, G. Gu, and J. Valentine, "Multifunctional metaoptics based on bilayer metasurfaces," Light: Sci. Appl. 8, 80 (2019).
- <sup>4</sup>Y. Zhou, I. I. Kravchenko, H. Wang, J. R. Nolen, G. Gu, and J. Valentine, "Multilayer noninteracting dielectric metasurfaces for multiwavelength metaoptics," Nano Lett. 18, 7529–7537 (2018).
- <sup>5</sup>M. Li, S. Li, L. K. Chin, L. K. Chin, Y. Yu, Y. Yu, D. P. Tsai, R. Chen, and R. Chen, "Dual-layer achromatic metalens design with an effective Abbe number," Opt. Express 28, 26041–26055 (2020).
- <sup>6</sup>C. R. Ocier, C. A. Richards, D. A. Bacon-Brown, Q. Ding, R. Kumar, T. J. Garcia, J. van de Groep, J.-H. Song, A. J. Cyphersmith, A. Rhode, A. N. Perry, A. J. Littlefield, J. Zhu, D. Xie, H. Gao, J. F. Messinger, M. L. Brongersma, K. C. Toussaint, L. L. Goddard, and P. V. Braun, "Direct laser writing of volumetric gradient index lenses and waveguides," Light: Sci. Appl. 9, 196 (2020).
- gradient index lenses and waveguides," Light: Sci. Appl. 9, 196 (2020).

  7D. Choudhury, J. R. Macdonald, and A. K. Kar, "Ultrafast laser inscription: Perspectives on future integrated applications," Laser Photonics Rev. 8, 827–846 (2014).
- <sup>8</sup>B. C. Stuart, M. D. Feit, S. Herman, A. M. Rubenchik, B. W. Shore, and M. D. Perry, "Optical ablation by high-power short-pulse lasers," J. Opt. Soc. Am. B 13, 459 (1996).

- <sup>9</sup>M. Lenzner, J. Krüger, S. Sartania, Z. Cheng, C. Spielmann, G. Mourou, W. Kautek, and F. Krausz, "Femtosecond optical breakdown in dielectrics," Phys. Rev. Lett. **80**, 4076–4079 (1998).
- <sup>10</sup>K. Miura, J. Qiu, H. Inouye, T. Mitsuyu, and K. Hirao, "Photowritten optical waveguides in various glasses with ultrashort pulse laser," Appl. Phys. Lett. 71, 3329–3331 (1997).
- <sup>10</sup>O. Tokel, A. Turnalı, G. Makey, P. Elahi, T. Çolakoğlu, E. Ergeçen, Ö. Yavuz, R. Hübner, M. Z. Borra, I. Pavlov, A. Bek, R. Turan, D. K. Kesim, S. Tozburun, S. Ilday, and F. Ö. Ilday, "In-chip microstructures and photonic devices fabricated by nonlinear laser lithography deep inside silicon," Nat. Photonics 11, 639 (2017).
- <sup>12</sup>G. Panusa, Y. Pu, J. Wang, C. Moser, and D. Psaltis, "Photoinitiator-free multiphoton fabrication of compact optical waveguides in polydimethylsiloxane," Opt. Mater. Express 9, 128 (2019).
- <sup>13</sup>W.-H. Yuan, J.-M. Lv, C. Cheng, X.-T. Hao, and F. Chen, "Waveguides and proportional beam splitters in bulk poly(methyl methacrylate) produced by direct femtosecond-laser inscription," Opt. Mater. 49, 110–115 (2015).
- <sup>14</sup>W. M. Pätzold, A. Demircan, and U. Morgner, "Low-loss curved waveguides in polymers written with a femtosecond laser," Opt. Express 25, 263–270 (2017).
- <sup>15</sup>N. D. Psaila, R. R. Thomson, H. T. Bookey, A. K. Kar, N. Chiodo, R. Osellame, G. Cerullo, A. Jha, and S. Shen, "Er:Yb-doped oxyfluoride silicate glass waveguide amplifier fabricated using femtosecond laser inscription," Appl. Phys. Lett. 90, 131102 (2007).
- <sup>16</sup>K. M. Davis, K. Miura, N. Sugimoto, and K. Hirao, "Writing waveguides in glass with a femtosecond laser." Opt. Lett. 21, 1729 (1996).
- glass with a femtosecond laser," Opt. Lett. 21, 1729 (1996).

  17 T. D. Gerke and R. Piestun, "Aperiodic volume optics," Nat. Photonics 4, 188–193 (2010).
- <sup>18</sup>T. D. Gerke and R. Piestun, "Aperiodic computer-generated volume holograms improve the performance of amplitude volume gratings," Opt. Express 15, 14954–14960 (2007).
- <sup>19</sup>R. R. Thomson, A. K. Kar, and J. Allington-Smith, "Ultrafast laser inscription: An enabling technology for astrophotonics," Opt. Express 17, 1963–1969 (2009).
- 20S. Gross and M. J. Withford, "Ultrafast-laser-inscribed 3D integrated photonics: Challenges and emerging applications," Nanophotonics 4, 332–352 (2015).
- <sup>21</sup>D. Tan, X. Sun, and J. Qiu, "Femtosecond laser writing low-loss waveguides in silica glass: Highly symmetrical mode field and mechanism of refractive index change," Opt. Mater. Express 11, 848–857 (2021).
- <sup>22</sup>G. E. Madden, D. Choudhury, W. N. MacPherson, and R. R. Thomson, "Development of low-loss mid-infrared ultrafast laser inscribed waveguides," Opt. Eng. 56, 075102 (2017).
- <sup>23</sup>C. R. Ocier, N. A. Krueger, W. Zhou, and P. V. Braun, "Tunable visibly transparent optics derived from porous silicon," ACS Photonics 4, 909–914 (2017).
- <sup>24</sup>C. R. Ocier, C. A. Richards, D. A. Bacon-Brown, N. A. Krueger, M. K. Clawson, J. A. N. T. Soares, and P. V. Braun, "Optically anisotropic porous silicon microlenses with tunable refractive indexes and birefringence profiles," Opt. Mater. Express 10, 868 (2020).
- <sup>25</sup>M. Mansouree, H. Kwon, E. Arbabi, A. McClung, A. Faraon, and A. Arbabi, "Multifunctional 2.5D metastructures enabled by adjoint optimization," Optica 7, 77–84 (2020).
- <sup>26</sup>R. R. Thomson, T. A. Birks, S. G. Leon-Saval, A. K. Kar, and J. Bland-Hawthorn, "Ultrafast laser inscription of an integrated photonic lantern," Opt. Express 19, 5698–5705 (2011).
- <sup>27</sup>S. G. Leon-Saval, "Photonic lantern," in Advanced Photonics 2015 (OSA, Boston, MA, 2015), p. NeS2D.2.
- <sup>28</sup>I. Spaleniak, N. Jovanovic, S. Gross, M. J. Ireland, J. S. Lawrence, and M. J. Withford, "Integrated photonic building blocks for next-generation astronomical instrumentation II: The multimode to single mode transition," Opt. Express 21, 27197–27208 (2013).
- <sup>29</sup>R. T. Chen, "Polymer-based photonic integrated circuits," Opt. Laser Technol. 25, 347–365 (1993).
- <sup>30</sup>A. Baum, P. J. Scully, W. Perrie, D. Liu, and V. Lucarini, "Mechanisms of femtosecond laser-induced refractive index modification of poly(methyl methacrylate)," J. Opt. Soc. Am., B 27, 107–111 (2010).

- <sup>31</sup>A. Baum, P. J. Scully, M. Basanta, C. L. P. Thomas, P. R. Fielden, N. J. Goddard, W. Perrie, and P. R. Chalker, "Photochemistry of refractive index structures in poly(methyl methacrylate) by femtosecond laser irradiation," Opt. Lett. 32, 190–192 (2007).
- <sup>32</sup>W. M. Pätzold, C. Reinhardt, A. Demircan, and U. Morgner, "Cascaded-focus laser writing of low-loss waveguides in polymers," Opt. Lett. 41, 1269–1272 (2016).
- <sup>33</sup>R. Infuehr, N. Pucher, C. Heller, H. Lichtenegger, R. Liska, V. Schmidt, L. Kuna, A. Haase, and J. Stampfl, "Functional polymers by two-photon 3D lith-ography," Appl. Surf. Sci. 254, 836–840 (2007).
- <sup>34</sup>X. Huang, Q. Guo, D. Yang, X. Xiao, X. Liu, Z. Xia, F. Fan, J. Qiu, and G. Dong, "Reversible 3D laser printing of perovskite quantum dots inside a transparent medium." Nat. Photonics 14, 82–88 (2020).
- parent medium," Nat. Photonics 14, 82–88 (2020).

  35A. J. Littlefield, D. Xie, C. A. Richards, J. Huang, M. L. Holley, U. Purakayastha, C. R. Ocier, P. G. Kwiat, P. V. Braun, and L. L. Goddard, "Low loss fiber-coupled volumetric interconnects fabricated via direct laser writing," (unpublished).
- <sup>36</sup>See https://www.comsol.com/model/step-index-fiber-bend-14189 for "Step-Index Fiber Bend," COMSOL (accessed 2021).
- <sup>37</sup>Y.-Y. Zhao, Y.-L. Zhang, M.-L. Zheng, X.-Z. Dong, X.-M. Duan, and Z.-S. Zhao, "Three-dimensional Luneburg lens at optical frequencies," Laser Photonics Rev. 10, 665–672 (2016).
- <sup>38</sup>A. J. Littlefield, C. A. Richards, C. R. Ocier, D. Xie, H. Gao, P. V. Braun, and L. L. Goddard, "Gradient index subsurface micro-optics," in Conference on Lasers Electro-Optics (CLEO), Paper No. FW2N.1 (2021).
- <sup>39</sup>B. H. Kleemann, M. Seesselberg, and J. Ruoff, "Design concepts for broadband high-efficiency DOEs," J. Eur. Opt. Soc. 3, 08015 (2008).
- 40J. Zhu and L. L. Goddard, "All-dielectric concentration of electromagnetic fields at the nanoscale: The role of photonic nanojets," Nanoscale Adv. 1, 4615–4643 (2019).
- <sup>41</sup>D. Jalas, A. Petrov, M. Eich, W. Freude, S. Fan, Z. Yu, R. Baets, M. Popović, A. Melloni, J. D. Joannopoulos, M. Vanwolleghem, C. R. Doerr, and H. Renner, "What is—and what is not—an optical isolator," Nat. Photonics 7, 579–582 (2013).
- <sup>42</sup>X. Xu, A. Broussier, T. Ritacco, M. Nahra, F. Geoffray, A. Issa, S. Jradi, R. Bachelot, R. Bachelot, R. Bachelot, C. Couteau, C. Couteau, S. Blaize, and S. Blaize, "Towards the integration of nanoemitters by direct laser writing on optical glass waveguides," Photonics Res. 8, 1541–1550 (2020).
- 43 M. del Pozo, C. Delaney, C. W. M. Bastiaansen, D. Diamond, A. P. H. J. Schenning, and L. Florea, "Direct laser writing of four-dimensional structural color microactuators using a photonic photoresist," ACS Nano 14, 9832–9839 (2020).
- 44M. Mastenbroek, "EUV industrialization high volume manufacturing with NXE3400B." Proc. SPIE 10809, 1080904 (2018).
- <sup>45</sup>X. Chen, W. Liu, B. Dong, J. Lee, H. O. T. Ware, H. F. Zhang, and C. Sun, "High-speed 3D printing of millimeter-size customized aspheric imaging lenses with sub-7 nm surface roughness," Adv. Mater. 30, 1705683 (2018).
- <sup>46</sup>L. Yang, A. El-Tamer, U. Hinze, J. Li, Y. Hu, W. Huang, J. Chu, and B. N. Chichkov, "Parallel direct laser writing of micro-optical and photonic structures using spatial light modulator," Opt. Lasers Eng. 70, 26–32 (2015).
- 47J. K. Hohmann, M. Renner, E. H. Waller, and G. von Freymann, "Three-dimensional μ-printing: An enabling technology," Adv. Opt. Mater. 3, 1488–1507 (2015).
- <sup>48</sup>H. Ning, N. A. Krueger, X. Sheng, H. Keum, C. Zhang, K. D. Choquette, X. Li, S. Kim, J. A. Rogers, and P. V. Braun, "Transfer-printing of tunable porous silicon microcavities with embedded emitters," ACS Photonics 1, 1144–1150 (2014).
- <sup>49</sup>R. Zhang, H. Ning, N. A. Krueger, D. Bacon-Brown, and P. V. Braun, "3D holographic photonic crystals containing embedded functional features," Adv. Opt. Mater. 4, 1533–1540 (2016).
- 50G. Korotcenkov and E. Rusu, "How to improve the performance of porous silicon-based gas and vapor sensors? Approaches and achievements," Phys. Status Solidi A 216, 1900348 (2019).